Hyperfine Interactions 123/124 (1999) 781–808

Experimental aspects of inelastic nuclear resonance scattering

A.I. Chumakov [a] and W. Sturhahn [b]

[a] *European Synchrotron Radiation Facility, BP 220, F-38043 Grenoble, France*
[b] *Advanced Photon Source, Argonne National Laboratory, Argonne, IL 60439, USA*

We present an introduction to the technique of inelastic nuclear scattering. The details of experimental setup, instrumentation, and measuring procedure are discussed. The typical appearance of experimental results and a brief description of data treatment methods are illustrated by examples of recent studies. Finally, the scope of information on lattice dynamics that is accessible with inelastic nuclear scattering is outlined.

1. Introduction

Inelastic nuclear resonance scattering is a new technique to study lattice dynamics. In contrast to other relevant methods like inelastic neutron, X-ray, and Raman scattering, inelastic nuclear scattering does not deal with phonon dispersion relations but, complementary to that, gives direct access to the density of phonon states (DOS). Despite having been developed only for the last few years [1–3], the technique has already found many applications [4,5]. The rapid development became possible due to several distinct advantages of the new method. First, it benefits from the resonant nature of interaction. The amplitude of resonance scattering scales with the radiation wavelength. For 10–30 keV X-rays this gives a several-orders-of-magnitude increase relative to, e.g., electronic Rayleigh scattering, where the scattering amplitude is proportional to the free electron radius. Therefore the count rate of inelastic nuclear scattering is large enough to perform a complete measurement in several hours. Furthermore, the large scattering cross-section allows investigation of lattice dynamics with very thin ($\sim$10 μm) samples. The combination of the large scattering cross-section and the small size of the synchrotron radiation beams ($\sim$mm^2) allows the use of tiny samples, typically of about few milligrams and the study of ultrathin films [5–8] and materials that are not available in large quantity (e.g., nanoparticles [9,10]).

Second, inelastic nuclear scattering does not necessarily require single crystal samples. It can also be carried out with polycrystalline, disordered, and amorphous materials. Even liquid [11] or gaseous [12] samples are accessible. This removes limitations on the aggregate phase and allows investigation of lattice dynamics during a phase or structural transformation [13].

Finally, inelastic nuclear scattering directly provides data on the density of phonon states. In contrast to, e.g., coherent inelastic neutron and X-ray scattering, no theoretical model has to be invoked. The data treatment resembles that for incoherent inelastic neutron scattering. However, as opposed to the latter technique, averaging over phonon momenta is not achieved by the specific location of detectors. The ideal "momentum-integrated" feature of inelastic nuclear scattering is assured by monitoring the yield of the nonradiative channel of nuclear de-excitation, where emitted atomic fluorescent radiation does not enter the momentum conservation law. Furthermore, the instrumental function of high-resolution monochromators is constant, and the energy transfer scale is defined with high precision. Therefore, even variations of the density of states of only a few percent can be accurately determined [14], whereas for, e.g., inelastic neutron scattering this is less than the standard deviation [15].

By definition, inelastic nuclear scattering is only sensitive to the vibrations of atoms with Mössbauer nuclei, which imposes a certain limitation on the accessible materials. On the other hand, it gives a useful feature of site selectivity. The technique provides a partial density of phonon states for the selected atoms of a crystal lattice. Isotope selectivity simplifies the data, especially for macromolecules [4,16,17] and proteins [18–20]. In addition, with a slight modification of the method, one may use the same experimental setup for nuclear resonant energy analysis of inelastic X-ray scattering [21]. A combination of the two methods provides a comparison between the "site-averaged" lattice dynamics and "site-selective" dynamics of the specific atoms [18–20].

This paper focuses on experimental aspects of the new technique. In particular, we discuss the experimental setup, instrumentation, electronics, and measuring procedure. We analyze the typical appearance of the experimental data and give a short introduction to the relevant theory and the methods of data treatment. Finally, we outline the scope of information on lattice dynamics that is accessible with inelastic nuclear scattering.

2. Instrumentation

Measurements of inelastic nuclear scattering require synchrotron radiation of high brightness and high spectral density. Therefore, such measurements are feasible mainly at third-generation sources of synchrotron radiation. At present, the experiments are concentrated at the two dedicated beamlines: the Nuclear Resonance beamline [16,22] at the European Synchrotron Radiation Facility (ESRF) in France and the 3ID beamline [23,24] at the Advanced Photon Source (APS) at Argonne National Laboratory in the USA. Recently the Nuclear Resonance beamline [25] at the SPring-8 facility in Japan came into operation. Measurements of inelastic nuclear scattering utilize the pulsed time structure of synchrotron radiation, thus they require special timing modes [26] of storage ring operation with large time intervals between pulses.

A typical experimental setup of a nuclear resonance beamline is shown in figure 1. More details can be found in the beamlines descriptions [16,22–25]. A synchrotron

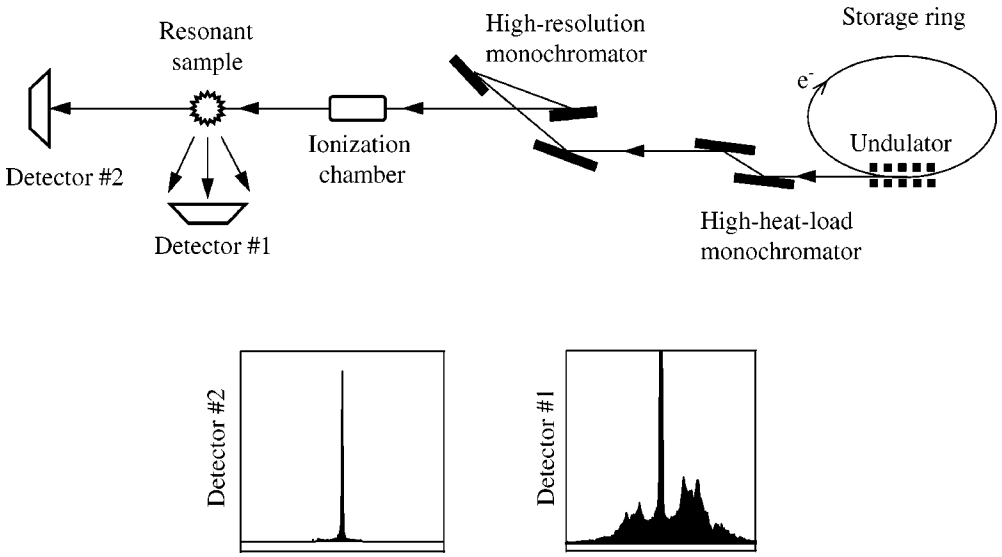

Figure 1. Experimental setup for measurements of inelastic nuclear scattering.

radiation beam is produced by an undulator inserted into the storage ring. The beam is monochromatized in two stages. In the first stage, the bandwidth is reduced down to a few eV by a high-heat-load monochromator. The monochromator is composed of two independent crystals (silicon at the ESRF and SPring-8, diamonds at the APS), which must be efficiently cooled. The monochromator has to sustain the intense X-ray beam and to transmit the radiation components in the vicinity of the nuclear transition with the maximal throughput. In the second stage, the bandwidth is reduced down to a few meV by a high-resolution monochromator [27,28]. A narrow energy bandpass is achieved with high-order reflection, which provides large energy–angle dispersion and has small angular acceptance. Sufficiently high throughput is achieved using the preceding asymmetric reflection, which collimates the incident synchrotron radiation beam in order to match the small angular acceptance of the subsequent crystal. As opposed to a high-heat-load monochromator, the high-resolution monochromator requires a separate set of crystals for each nuclear transition. Because a gain in energy resolution is often achieved at the expense of loss in throughput, the actual choice of the high-resolution monochromator should be adjusted to the particular experiment. More details on high-resolution monochromators can be found in [27].

After the high-resolution monochromator, the beam passes through an ionization chamber, which monitors the flux of incident radiation, irradiates a sample and excites the resonant nuclei. Scattered radiation is counted by two avalanche photodiode (APD) detectors [29]. The first detector is located close to the sample and counts the quanta scattered in a large solid angle. The second detector is located far away from the sample and counts the quanta scattered by the nuclei in the forward direction.

The two detectors monitor different processes of nuclear scattering. Being scattered inelastically, the quantum acquires a certain phase shift and, therefore, is no longer coherent with the incident radiation. If the phase shift is random for various nuclei, the scattering is spatially incoherent, and the scattered quanta may be associated with some particular nucleus. The products of de-excitation are emitted as a spherical wave (neglecting the polarization effects). The intensity of incoherent nuclear scattering, which may proceed both elastically and inelastically, is monitored by the first detector. In order to collect a sufficient flux, the detector should cover a large solid angle; therefore it is placed close to the sample. At ambient conditions, the sensitive area of the detector can be located at about 1 mm from the sample, covering about a quarter of a complete sphere. Measurements at variable temperatures require special inserts for cryostats and furnaces, which allow one to keep the distance between the sample and the detector small but with a good thermal insulation between them.

The second detector monitors nuclear forward scattering. In order to avoid a contribution of incoherent scattering, the detector is located far from the sample. The paths of the waves scattered by various nuclei in the forward direction are indistinguishable, therefore all waves have the same phases and the scattering is spatially coherent. The scattered quantum cannot be associated with a particular nucleus but is a result of collective scattering by the nuclear ensemble. This is an elastic process, because any local energy transfer would destroy the coherence. Thus the second detector measures the intensity of coherent forward nuclear scattering, which proceeds elastically.

Figure 1 shows a typical appearance of the data, measured by the two detectors. The intensity of incoherent (detector #1) and coherent (detector #2) scattering is measured as a function of the incident radiation energy, which is determined by the angular positions of the crystals in the high-resolution monochromator. Coherent scattering proceeds elastically, hence it appears only when the energy of the incident radiation coincides with the energy of a nuclear transition. The data provide the instrumental function of the high-resolution monochromator, because the width of the nuclear transition on this scale is negligible. In particular, the peak gives a precise indication of the energy position of nuclear resonance. Incoherent scattering, in addition to the central elastic peak, has a certain probability outside the nuclear resonance. This part corresponds to inelastic nuclear scattering accompanied by the creation or annihilation of phonons.

Precise monitoring of the instrumental function in *parallel* with the main measurements is extremely important for the subsequent data processing. A Fourier image of the instrumental function is required for the de-convolution procedure [30,31]. Several moments of the instrumental function are required in order to apply the sum rules [2,30–32]. Due to instabilities of crystal temperature and beam position the instrumental function may vary slightly during the experiment. Therefore, if permanent monitoring of the experimental function is difficult (e.g., because of a thick sample), it should be frequently monitored between the measurements using another appropriate resonant absorber.

Comparing the instrumentation of inelastic nuclear scattering with that of, e.g., inelastic neutron or X-ray scattering, one may note that the setup for inelastic nuclear scattering benefits from the narrow width of the nuclear resonance. Other inelastic techniques deal twice with the problem of monochromatization: a highly monochromatic beam has to be prepared to irradiate the sample, and the energy of the scattered radiation has to be analyzed. Then the energy transfer is determined as a difference between the energy of scattered and incident radiation. In inelastic nuclear scattering, the narrow width of nuclear levels ($\sim$ neV) makes the nuclear resonance itself an ideal energy reference. Therefore, the analyzer section of the traditional inelastic scattering setup may be omitted. The energy transfer is determined as a shift of the incident energy relative to the energy of the nuclear transition, which is indicated by the elastic peak in the incoherent spectrum and by the peak of the nuclear forward scattering.

3. Measurements

In order to obtain the energy spectrum of inelastic nuclear scattering, the quanta of nuclear scattering have to be distinguished from other quanta that pass through the sample without interaction or that are scattered by electrons. This is achieved by using the pulsed time structure of synchrotron radiation. The quanta of nuclear scattering are delayed due to the finite lifetime of the nuclear excited state, whereas the electronic scattering is essentially prompt on that time scale. Fast electronics is synchronized with the revolutions of the electron beam in the storage ring and only counts the events between the pulses of synchrotron radiation. Therefore only the delayed quanta, which result from nuclear scattering, are detected.

Figure 2 shows a block circuit of the electronics. Because the channels for both detectors are identical, only one of them is shown. The detectors should be able to sustain an intense pulses of prompt scattering (up to 10^9 photons/s) during the flash of synchrotron radiation and several nanoseconds later to detect a single delayed quantum of nuclear scattering. Only a few detectors can meet these severe requirements. At present the best performance is achieved with large-area avalanche photodiodes (APD) detectors [29]. The signal from the detector is supplied to two constant-fraction discriminators (CFD). The first discriminator transmits all incoming signals. Therefore the corresponding counter acquires the count rate of overall scattering, which is dominated by the prompt electronic scattering channel. The second discriminator is controlled by a veto signal from a bunch-clock. It does not allow the signal to pass during the pulses of synchrotron radiation. Therefore the second counter only accepts the counts of the delayed nuclear scattering. A proper synchronization of the veto signal with synchrotron radiation pulses is achieved by monitoring the time distribution of scattering. The time spectrum of scattering is measured using a time–amplitude converter (TAC) and a multichannel analyzer (MCA).

A typical time distribution of nuclear scattering is shown in figure 3. The time dependence of incoherent nuclear scattering contains information on the hyperfine structure of the nuclear transition [33] and on the balance of radiative and nonradiative

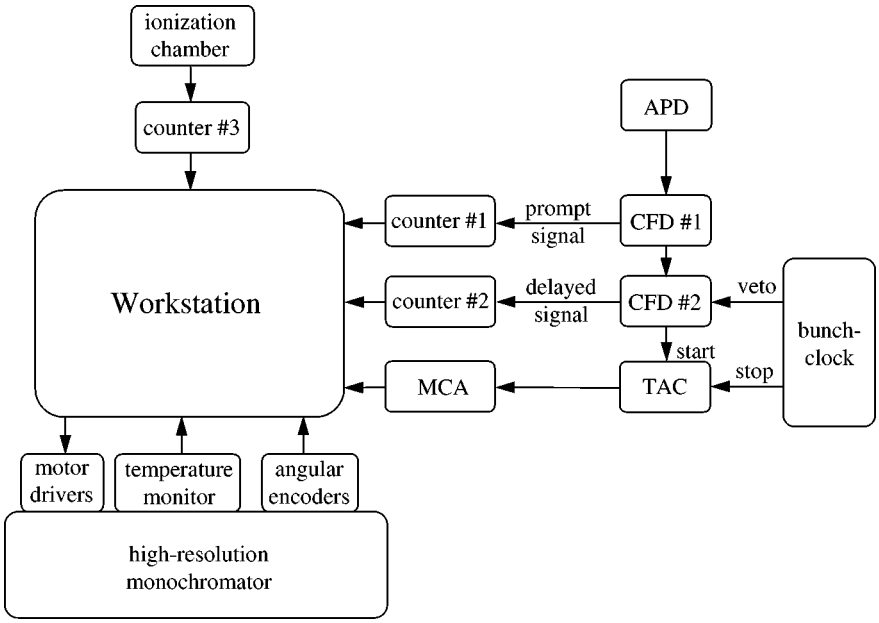

Figure 2. Block circuit of the electronics for measurements of inelastic nuclear scattering. APD – avalanche photodiode detector; CFD – constant fraction discriminator; TAC – time-amplitude converter; MCA – multichannel analyzer.

channels of nuclear scattering [34]. For studies of lattice dynamics, however, the details of the time distribution are not important [35]. Here the purpose is to collect the time-integrated flux of incoherent nuclear scattering, to avoid counting the prompt peak of electronic scattering at zero time and to assure that the measured signal is proportional to the inelastic absorption cross-section. The latter requirement compels one to increase the width of the veto signal in order to exclude from the collected signal not only the prompt scattering but also the delayed nuclear scattering in the first $\sim$10 ns after the prompt pulse. The reason is that at high count rates the constant fraction discriminators can suffer saturation effects, where the count rate in the first $\sim$10 ns is not linear in the scattered intensity. Careful elimination of this effect must be achieved.

The longer veto signal also allows one to decrease the relative contribution of the central elastic peak, which is useful because the tails of the central peak hide inelastic scattering for low energy transfer. Figure 3 shows that the time distributions of nuclear scattering at resonance and off resonance are different. Inelastic excitation of nuclei off resonance leads to an exponential decay of nuclear scattering with a decay time equal to or slightly longer than the natural lifetime [34] (figure 3(a)). However, when the energy of the incident radiation coincides with that of the nuclear transition, nuclear excitation may proceed elastically, which leads to nuclear forward scattering. The intensity of the forward scattered wave is strongly enhanced relative to incoherent scattering [36], especially just after the prompt pulse. Subsequent nuclear

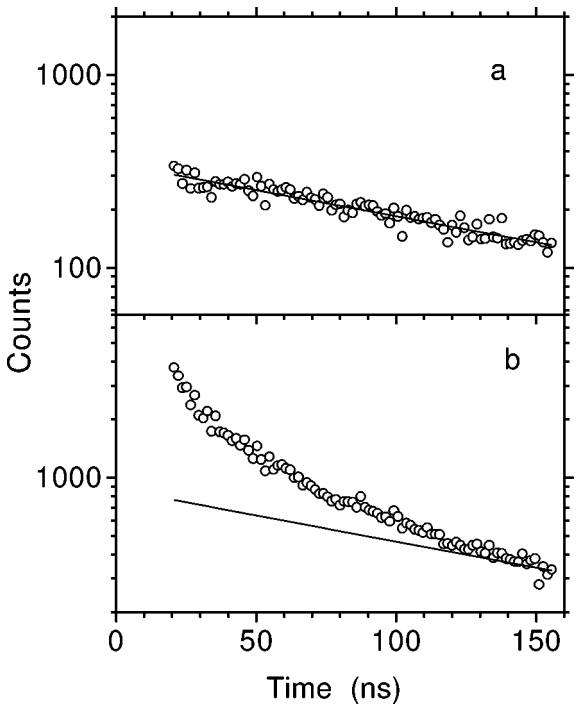

Figure 3. Time evolution of emission of the 6.4 keV K_α atomic fluorescent radiation after excitation of the ^{57}Fe nuclei by a pulse of synchrotron radiation (a) out of resonance and (b) in resonance. The solid line shows the fit to the out-of-resonance data with an exponent and a constant background with the obtained decay time of 156 ± 5 ns. The same line is also shown at the lower part for comparison.

and electronic rescattering of the forward wave influences the incoherent channel of scattering as well [37,38]. Therefore, the decay of incoherent nuclear scattering is much faster at resonance (figure 3(b)). A moderate increase of the veto signal width allows exclusion of an essential part of the incoherent scattering at resonance while keeping almost the same count rate off resonance.

The intensity of incoherent scattering should be measured as a function of the incident radiation energy. The procedure for an energy scan is performed by prescribed movement of the crystals of the high-resolution monochromator. The energy of the delivered radiation is mainly determined by the crystal with the smallest energy bandwidth. If the energy bandwidth of other reflections is much larger, then the energy scan may be performed by rotation of only this crystal. This is not the case for the most recent monochromators with ultra-high energy resolution, where two successive reflections have the same Miller indices [39,40]. In this case, the upstream (along the X-ray beam) crystal should be rotated with an angular velocity twice slower than the downstream one. Furthermore, these monochromators deliver X-ray beams of different energies at slightly different angles relative to the horizontal plane. Therefore the beam moves vertically during the energy scan. In order to avoid a variation of the scattered intensity, the sample

should preferably be located closer to the high-resolution monochromator and/or a vertical motion of the sample should be included in the energy scanning procedure.

The typical angular displacement of crystals during a single step of the energy scan is $\sim$0.1 μrad. In practice, the mechanics cannot always fulfill such a small motion precisely enough. Therefore the angular displacement of the crystals has to be monitored by high-precision angular encoders. The change in the delivered energy ΔE is connected with the angular displacement of the crystals, $\Delta\theta$, by Bragg's law, which displacement is related to the temperature-dependent lattice constant of crystals. Due to the very high energy resolution ($E/\Delta E \sim 10^7$) of the monochromator, the energy of the delivered radiation depends sensitively on the crystal temperature. For instance, an energy shift of one bandwidth ($\sim$0.9 meV) for the high-resolution monochromator reported in [40] may result from a $\sim$20 mK change of the crystal temperature. Therefore, the crystal temperature must be precisely stabilized and monitored. Corresponding corrections for temperature instability may be included in the data evaluation procedure [27].

Despite the high intensity of incoherent nuclear scattering, one energy scan may last a relatively long time (e.g., about an hour). Therefore, one has to take into account a variation of X-ray beam intensity due to a decay of the electron beam in the storage ring and possible instabilities of crystal optics. For these purposes, the experimental data have to be normalized by some monitor signal. For forward-scattering data, normalization by a monitor signal from the ionization chamber (figure 1) is a good choice. For the incoherent scattering data, one should preferably use the prompt signal of incoherent scattering, because this also allows elimination of errors that result from possible displacements of the X-ray beam relative to the sample during the energy scan.[1] It is preferable to keep the time of a single energy scan relatively short and to accumulate the data in numerous scans. The separate scans can be added together using the simultaneously measured instrumental function as a center reference. The variation of the angular position of the instrumental function from scan to scan serves to estimate the instability of the crystal optics.

4. Inelastic nuclear scattering and absorption

Incoherent nuclear scattering consists of several types of radiation. In general, all of them may be chosen to study lattice vibrations. In practice, the choice is often determined by technical reasons. However, the information obtained may depend on the specific selection.

An excited nucleus can decay via two channels: radiative decay and internal conversion. Decaying via the radiative channel, the nucleus emits nuclear fluorescent radiation. The relative probability of this channel is $1/(1+\alpha)$, where α is the conversion coefficient. The energy of the emitted γ-radiation may be precisely equal to

[1] This is applicable if the prompt scattering signal has no saturation effects.

the energy of the nuclear transition (elastic emission), or shifted by the energy of the accompanying phonon (inelastic emission). When the nucleus decays via the internal conversion channel, the energy of the nuclear excited state is transferred to an electron of the atomic shell. This conversion electron leaves the atom, and the remaining hole results in the subsequent emission of atomic fluorescent radiation and/or Auger electrons. The relative probability of this channel is $\alpha/(1+\alpha)$. Since for most of the Mössbauer isotopes $\alpha > 1$, internal conversion is the dominating channel.

Above we have used the expression "scattering" for both channels of nuclear decay. Because two channels might be differently influenced by lattice dynamics, it is worthwhile to distinguish them explicitly. In this section we reserve the expression "scattering" for the radiative channel, where the absorbed photon results in a re-emitted γ-ray, whereas for the non-radiative channel we use the expression "absorption".

The choice of a particular radiation allows one to study specifically either inelastic nuclear *absorption* or inelastic nuclear *scattering*. If the products of internal conversion are detected (atomic fluorescent radiation, conversion or Auger electrons), one measures the cross-section of inelastic nuclear absorption. The location of the detector relative to the incident beam does not matter, because the angular distribution of the atomic emission is an atomic property that does not depend on the "history" of nuclear excitation. Thus the allowed momentum transfer is not specified by the experimental setup. The phonons with any momentum allowed by the dispersion relations for a particular energy transfer contribute equally to nuclear absorption. Therefore, nuclear absorption provides an ideal "momentum-integrated" tool for the measurement of lattice dynamics.

If the nuclear fluorescent radiation of the radiative channel is detected (i.e., if one studies specifically inelastic "scattering"), the analysis becomes more complicated. The momentum transfer, which is defined by the specific location of the detector, and the energy of the scattered radiation must be considered.

Until now most of the reported studies were performed under experimental conditions in which atomic fluorescent radiation was the dominating contribution to the measured signal. This means that the studied channel was inelastic nuclear *absorption*. The contribution of nuclear fluorescent radiation is only a few percent for typical experimental conditions [34]. This is caused by the dominant probability of the internal conversion channel, the higher efficiency of the detectors for the softer atomic fluorescent radiation, and trapping of nuclear fluorescent radiation in the sample [34]. Conversion electrons and Auger electrons [38,41] also give information about inelastic nuclear absorption.

However, for several Mössbauer isotopes, monitoring atomic fluorescence is not feasible because of its low energy. In this case nuclear fluorescent radiation becomes the dominant product, and the studied channel is specifically nuclear resonance *scattering*. This, for instance, holds for ^{119}Sn. It was found that the energy spectrum of inelastic nuclear *scattering* from a polycrystalline ^{119}Sn sample [42] can be well described by a theory of inelastic nuclear *absorption*. Theoretical analysis showed that, if the integration over the angle of emission is complete, the energy spectra of

inelastic nuclear *absorption* and incoherent nuclear *scattering* differ only by a scaling factor [35]. The properties of *angular-resolved* inelastic nuclear *scattering* are not completely clear yet. This topic is especially interesting because it is related to the feasibility of *coherent inelastic nuclear scattering*. One may suppose that if the energy transfer is defined, the scattered γ-ray quanta should be emitted along the specific directions that are determined by the momentum transfer via phonon dispersion relations. However, in contrast to, e.g., neutron scattering, the characteristic time of nuclear scattering is much longer than the phonon lifetime. Therefore, although a large number of nuclei can be involved in the particular mode of lattice vibration, the coherence of the waves scattered by various nuclei is preserved only during a very short time. Then, in analogy to nuclear scattering under diffusion conditions [37,43], one may expect an extremely fast ($\sim 10^{-12}$ s) decay of coherent inelastic nuclear scattering, which would make its observation difficult.

5. Experimental data

An example of experimental data is given in figure 4. The energy dependence of inelastic nuclear absorption of synchrotron radiation in a polycrystalline α-iron sample at room temperature is shown as a function of energy of the incident radiation. The central peak corresponds to elastic nuclear absorption. The structure outside the central peak shows the spectrum of inelastic absorption, accompanied either by creation ($E > 0$) or by annihilation ($E < 0$) of phonons.[2] At ambient temperature one may recognize various contributions to the energy spectrum, which correspond to inelastic absorption accompanied by excitation or annihilation of different numbers of phonons. The normalized probability of inelastic nuclear absorption $W(E)$ can be decomposed in terms of a multiphonon expansion [44]:

$$W(E) = f_{\mathrm{LM}} \left(\delta(E) + \sum_{n=1}^{\infty} S_n(E) \right). \tag{5.1}$$

Here the Dirac δ-function $\delta(E)$ describes the elastic part of absorption (zero-phonon term), and the nth term of the series $S_n(E)$ represents the inelastic absorption accompanied by creation (annihilation) of n phonons. The one-phonon term is given by

$$S_1(E) = \frac{E_{\mathrm{R}} \cdot g(|E|)}{E \cdot (1 - \mathrm{e}^{-\beta E})}, \tag{5.2}$$

[2] Note that for inelastic nuclear scattering, the relative energy scale is defined as the energy of the incident radiation relative to the energy of the nuclear transition. This gives a positive sign of the energy transfer for the phonon creation part of the spectrum and a negative one for the annihilation part, which is contrary to definitions for, e.g., incoherent inelastic neutron scattering.

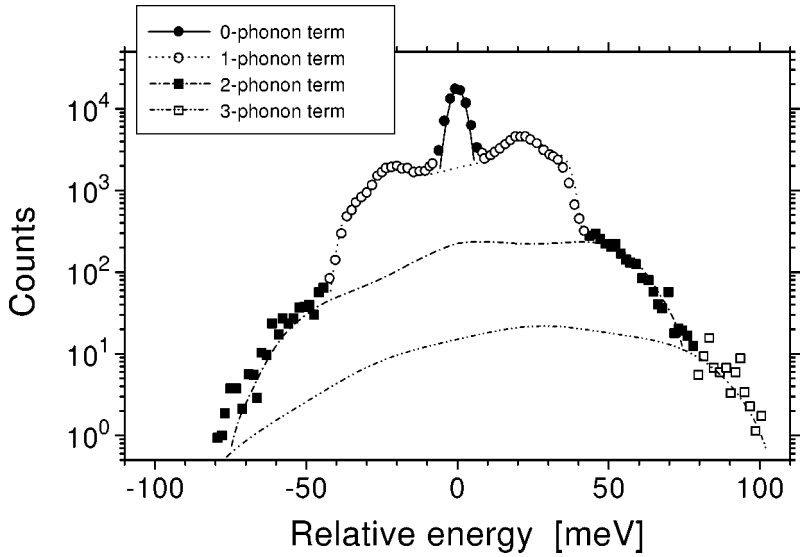

Figure 4. Expansion of the energy spectrum of inelastic nuclear absorption of synchrotron radiation in α-iron in multi-phonon terms. The data were taken at room temperature. Different markers show the regions of the spectra where the corresponding contributions are dominant. The lines are the calculations according to eqs. (5.1)–(5.3) with the density of phonon states obtained from neutron scattering [15] and convoluted with the instrumental function of the monochromator.

and the subsequent terms in the harmonic approximation may be found through the recursive relation

$$S_n(E) = \frac{1}{n}\int_{-\infty}^{\infty} S_1\big(E'\big) S_{n-1}\big(E - E'\big)\,\mathrm{d}E'. \tag{5.3}$$

Here $\beta = (k_\mathrm{B}T)^{-1}$ with k_B the Boltzmann constant, T is the temperature; $E_\mathrm{R} = \hbar^2k^2/2M$ – the recoil energy of a free nucleus; k – the wave vector of the X-ray quantum; M – the mass of the atom. The function $g(E)$ is the normalized density of phonon states

$$g(E) = V_0 \frac{1}{(2\pi)^3}\sum_j \int \mathrm{d}\vec{q}\,\delta\big[E - \hbar\omega_j\big(\vec{q}\big)\big], \tag{5.4}$$

where V_0 is the volume of the unit cell, the index j enumerates the branches of the dispersion relation $\hbar\omega_j(\vec{q})$, $\vec{q}$ is the phonon momentum, and the integral is taken in the first Brillouin zone. The detailed theory of inelastic nuclear absorption has been published in [30,35,44].

The relative contribution $\int S_n(E)\,\mathrm{d}E$ of the n-phonon term is given by $(-\ln f_\mathrm{LM})^n/n!$ [44]. If the Lamb–Mössbauer factor is close to unity, the expansion in eq. (5.1) converges rapidly, and only a few terms are significant. For instance, the contributions of the first three terms can be seen in figure 4, whereas higher order contributions are negligible. This easy distinction of the multi-phonon contributions is

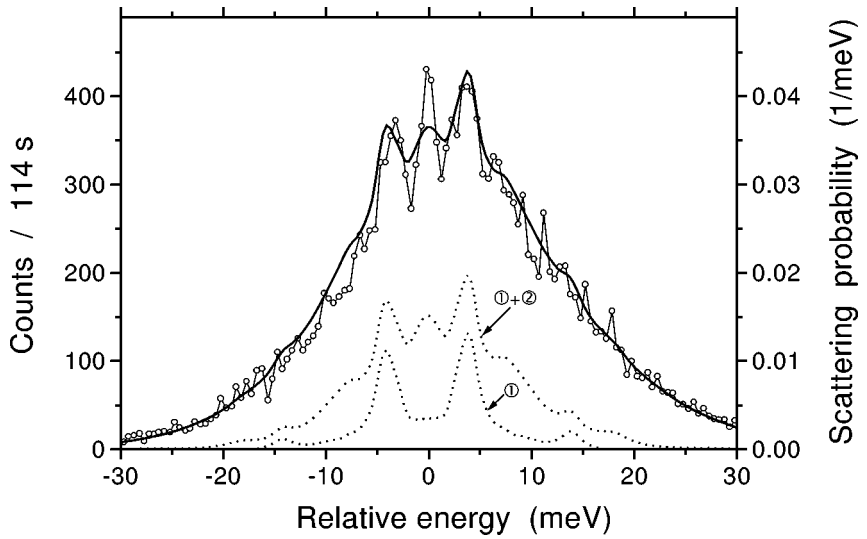

Figure 5. Energy spectrum of inelastic nuclear scattering of synchrotron radiation by a ^{119}Sn foil. The experimental data are shown by the open circles and the thin line (to guide the eye). The thick solid line shows the probability density of inelastic nuclear scattering, calculated using the density of phonon states from [45] according to eqs. (5.1)–(5.3) and convoluted with the instrumental function of the monochromator. The single-phonon contribution (①) and the sum of single- and two-phonon contributions (①+ ②) to the total probability of inelastic nuclear scattering are shown by the dotted lines. From [42].

no longer possible if the Lamb–Mössbauer factor is small. In this case the expansion eq. (5.1) converges slowly, and a large number of terms has to be taken into account. Figure 5 shows the energy spectrum of inelastic nuclear scattering in the polycrystalline β-Sn sample, which is dominated by a multi-phonon contribution [42]. An interpretation of the expansion eq. (5.1) as the sum of multi-phonon processes in this case becomes meaningless. The extraction of the density of phonon states from the experimental data is ambiguous or impossible under these conditions.

The energy spectrum of inelastic nuclear absorption satisfies the detailed balance rule, which means that for any particular energy the ratio of phonon creation and phonon annihilation probability is given by $\exp(\beta|E|)$. For the one-phonon term, the detailed balance is given by a factor $1/(1-\mathrm{e}^{-\beta E})$ (eq. (5.2)). For the higher order contributions, it can be checked with a recursive procedure. The detailed balance determines an asymmetry of the energy spectra, which becomes more pronounced at lower temperatures.

Figure 6 shows the temperature behaviour of the energy spectra of inelastic nuclear absorption in α-iron [14]. One may see that the phonon-annihilation part ($E < 0$) almost disappears at low temperature. The physical meaning of the detailed balance becomes clear when one notes that, for the phonon creation part, the factor $1/(1-\mathrm{e}^{-\beta E})$ is equivalent to $(n_\mathrm{B}+1)$ with the Bose occupation factor $n_\mathrm{B} = 1/(\exp^{\beta|E|}-1)$. The phonon annihilation part is proportional to n_B. At low temperature, the occupation

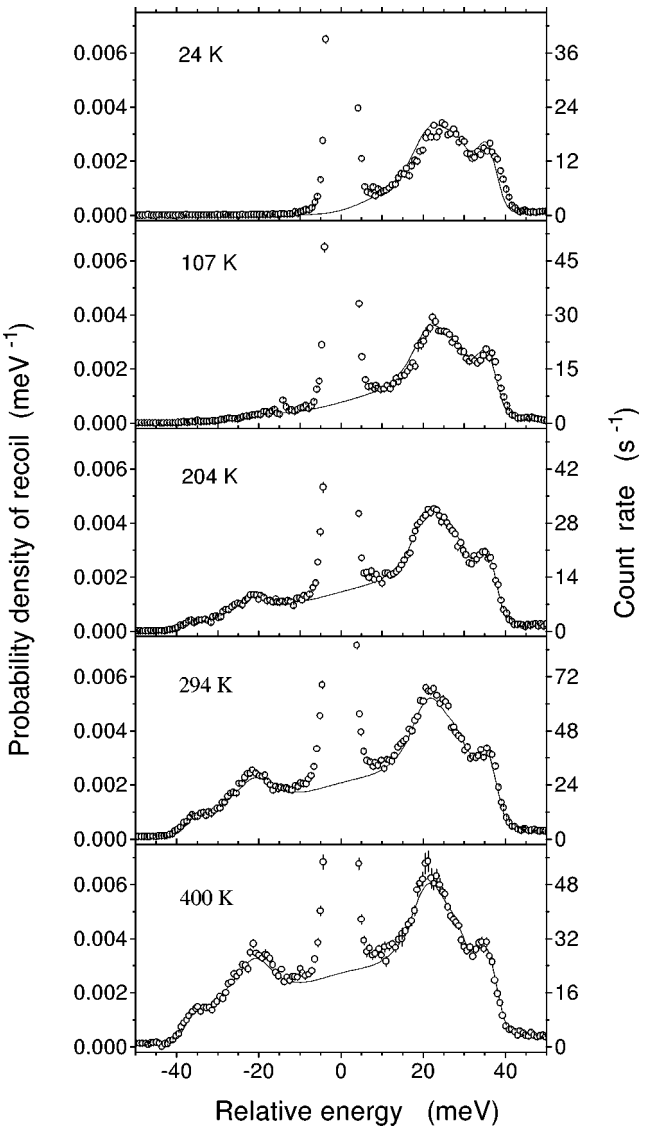

Figure 6. Energy spectra of inelastic nuclear absorption of synchrotron radiation by α-^{57}Fe at various temperatures. Solid lines are calculations according to eqs. (5.1)–(5.3), based on the results of neutron scattering at room temperature [15] and convoluted with the instrumental function of the monochromator. From [14].

factor vanishes, i.e., there are no phonons excited in the lattice. Therefore, an incident X-ray quantum cannot gain energy from lattice vibrations. However, it may still lose energy by creating new phonons.

At low temperatures, besides vanishing in the phonon-annihilation part, the energy spectrum of inelastic absorption also vanishes at the low energy transfer region in the

phonon-creation part [14,46]. One may easily show that at high temperature $S_1(E) \sim g(E)/E^2$, whereas at low temperature $S_1(E) \sim g(E)/E$. On the other hand, the behaviour of the density of states for most solids at low phonon energy may be well approximated by the Debye law $g(E) \sim E^2$. Therefore, inelastic absorption with low energy transfer approaches a constant level in a high-temperature approximation, but vanishes at low temperatures.

The energy dependence of inelastic nuclear absorption would be directly proportional to the probability $W(E)$, which is given by eq. (5.1), if the yield of atomic fluorescence is a linear function of the absorption cross-section. This holds for the inelastic part of the energy spectrum, because the cross-section of inelastic scattering is small (e.g., $\sim 10^{-25}$ cm^2 for ^{57}Fe). However, this is not valid for the central elastic peak. At resonance the irradiated volume becomes smaller due to the high cross-section of elastic absorption [2]. The saturation effect decreases the relative area of the central peak. On the other hand, at resonance the radiation wave field in the sample is modified by nuclear forward scattering, which increases the intensity of incoherent scattering and modifies its time distribution [37,38] (figure 3), therefore the relative area of the central peak depends on the width of the veto signal.

Thus, the area of the inelastic part of the energy spectrum is proportional to the recoil fraction of absorption, but the area of the central elastic peak is not proportional to the recoilless fraction. Therefore, the experimental data cannot be normalized according to an assumption of unit area. Another approach, which is based on sum rules, was developed in [2]. The normalization depends only on the shape of the inelastic part. According to Lipkin's sum rules [47,48], the first moment of the energy spectrum of inelastic absorption equals the mean recoil energy E_{R} of a free nucleus:

$$\int_{-\infty}^{\infty} W(E) E \, \mathrm{d}E = E_{\mathrm{R}}. \tag{5.5}$$

This property gives a direct normalization of the inelastic part of the absorption spectrum. The influence of the central peak is excluded, because it is essentially symmetric and does not contribute to the first moment. The corrections on the possible asymmetry of the instrumental function may also be taken into account [2].

6. Anisotropic inelastic absorption in single crystals

For the examples above, the orientation of the incident X-ray beam relative to the crystallographic directions of the sample is not important. This is justified for amorphous and polycrystalline samples [44]. However, it is not necessarily valid for single crystals, since vibrations along the various crystallographic directions may have different frequency spectra. It is well known, for instance, that in anisotropic single crystals the recoil fraction of nuclear absorption may depend on crystal orientation. A similar sensitivity to crystal orientation may also be expected for energy spectra of inelastic nuclear absorption.

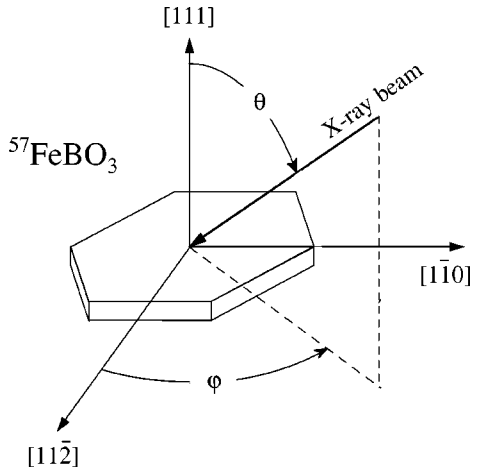

Figure 7. Orientation of the incident X-ray beam relative to the $^{57}FeBO_3$ crystal. From [49].

An example of anisotropic inelastic nuclear absorption is shown in figures 7 and 8. The measurements were performed with a ferric borate $^{57}FeBO_3$ single crystal, which has a calcite-type structure with a $R\bar{3}c$ space group. Energy spectra of inelastic nuclear absorption were measured for several polar angles θ and azimuthal angles φ between the incident X-ray beam and the [1 1 1] axis (figure 7). A pronounced dependence of the energy spectra on the polar angle was observed, whereas no significant dependence on the azimuthal angle was found [49]. The energy spectra of inelastic nuclear absorption for various polar angles are shown in figure 8. When the polar angle is large (figures 8(a), (b)), the spectra consist of one peak at about $\pm$20 meV in the energy-loss and energy-gain sides of the spectrum, respectively. When the angle decreases (figures 8(c)–(e)), this peak remains in the spectrum, but an additional peak appears at about $\pm$30 meV.

The theory of inelastic nuclear absorption for the case of an anisotropic single crystal was developed in [30]. It was shown that eqs. (5.1)–(5.3) hold for any orientation of the incident beam relative to the crystallographic axes. However, the conventional density of phonon states $g(E)$ defined by eq. (5.4) has to be substituted by a "projected" density of states $\tilde{g}(E)$, where the contributions of various phonons are weighted by projections of the phonon polarization vector $\vec{\mathbf{e}}_j(\vec{\mathbf{q}})$ in the direction of the X-ray beam $\vec{s} = \vec{k}/k$:

$$\tilde{g}(E, \vec{s}) = V_0 \frac{1}{(2\pi)^3} \sum_j \int \mathrm{d}\vec{q}\, \delta\big[E - \hbar\omega_j(\vec{q})\big] \big|\vec{s} \cdot \vec{e}_j(\vec{q})\big|^2. \tag{6.1}$$

Similarly to the conventional density of states, the "projected" DOS is normalized, and the Lipkin sum rules are valid for the energy spectra of inelastic nuclear absorption for every particular crystallographic direction [30].

The necessary conditions for polar and azimuthal anisotropy of inelastic nuclear absorption are discussed in [35], where the specific Bravais lattices, which allow a

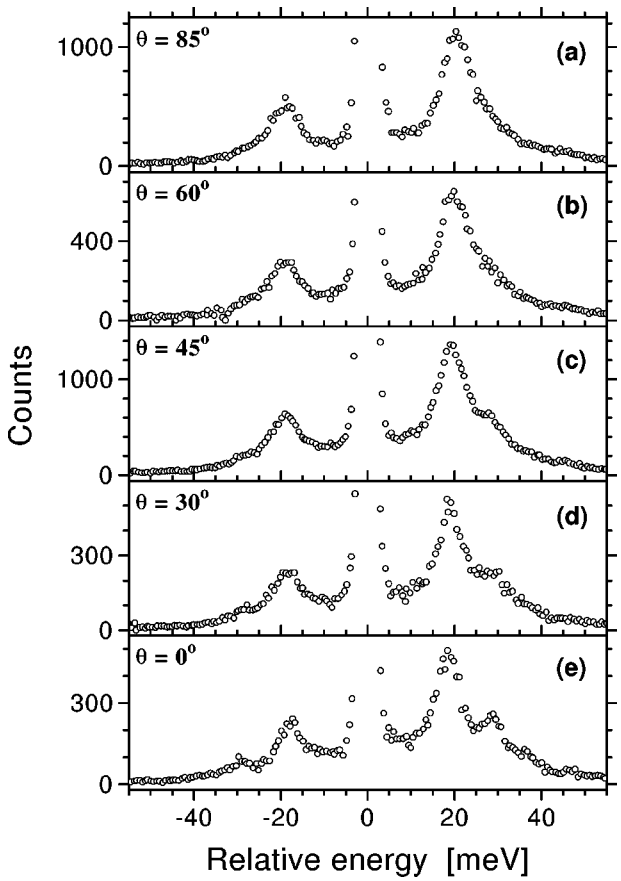

Figure 8. Energy spectra of inelastic nuclear absorption of synchrotron radiation in the $^{57}FeBO_3$ single crystal for various polar angles θ between the direction of the incident X-ray beam and the [1 1 1] axis. The azimuthal angle was kept constant ($\varphi = 90°$). From [49].

particular kind of anisotropy, are pointed out. Even if the crystal symmetry does allow the anisotropy of nuclear absorption, it may still vanish due to the specific basis of the unit cell. For instance, no definite anisotropic effect was observed for a hematite $^{57}Fe_2O_3$ crystal [50], although it has the same $R\bar{3}c$ space group as the ferric borate $^{57}FeBO_3$.

The anisotropy of energy spectra of inelastic nuclear absorption is not necessarily accompanied by the anisotropy of the Lamb–Mössbauer factor. The Lamb–Mössbauer factor may be expressed through the density of states as [44]

$$f_{\mathrm{LM}} = \exp\left(-E_{\mathrm{R}} \int_0^\infty \frac{g(E)}{E} \cdot \frac{1+\mathrm{e}^{-\beta E}}{1-\mathrm{e}^{-\beta E}}\,\mathrm{d}E\right). \tag{6.2}$$

According to eq. (6.2), the contribution of the lattice vibrations at various energies to the exponential argument is weighted by a factor of $1/E$ at low temperature, and by

a factor of $1/E^2$ at high temperature. This shows that the Lamb–Mössbauer factor is determined mainly by the low-energy part of the density of states, where for most solids it may be approximated by the Debye model. Therefore the Lamb–Mössbauer factor, especially at high temperature, is not very sensitive to the specific details of the density of phonon states. For instance, despite the pronounced anisotropy of the energy spectra of inelastic nuclear absorption in ferric borate crystal (figure 8), the Lamb–Mössbauer factor at room temperature does not show a significant angular dependence [49].

7. Examples of application

Applications of inelastic nuclear scattering benefit greatly from the absence of special requirements on the aggregate state of the investigated material. The technique may be applied to single crystalline, polycrystalline, disordered, and amorphous materials. A few demonstration experiments have been performed with liquid [11] and gaseous [12] samples. This flexibility gives an access to studies of phase and structural transformation.

Figure 9 shows an example of the structural transformation in an Fe_3Al alloy from a disordered to a partially ordered and a DO_3-ordered state [13]. The structural transformation changes the local chemical environment of the iron atoms. The energy spectra of nuclear inelastic absorption systematically follow this variation. The spectra consequently lose fine structure during the transformation of the alloy to the disordered state. For instance, the sharp peak at about 40 meV almost disappears for the disordered

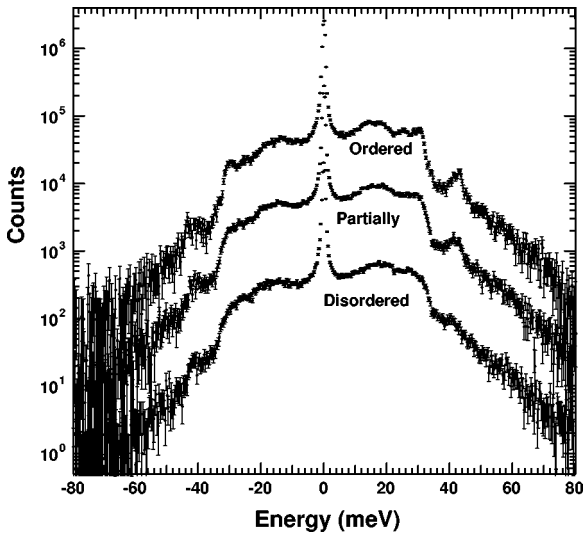

Figure 9. Energy spectra of inelastic nuclear absorption of synchrotron radiation in disordered, partially ordered, and ordered $^{57}Fe_3Al$ alloys. Data for partially ordered and ordered samples are shifted vertically by factors of 10 and 100, respectively. From [13].

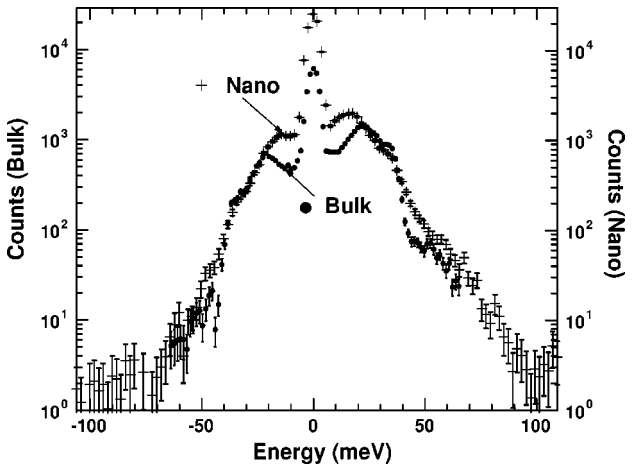

Figure 10. Energy spectra of inelastic nuclear absorption of synchrotron radiation in a bulk ^{57}Fe foil and ballistically consolidated nanocrystalline ^{57}Fe particles of about 10 nm size. Data are shown with equal intensity at 25 meV. From [9].

sample. The changes were modeled by assigning vibrational spectra to iron atoms in different first-nearest-neighbour chemical environments.

Another significant advantage of inelastic nuclear scattering is the small amount of material required. This opens, for instance, the possibility to investigate very thin films of resonant isotopes [5–8]. In order to increase the count rate, one can additionally benefit from the wave-guide effect by covering the film of the resonant isotope with a layer of another material. This structure causes a "capture" of the wave field inside the film of the resonant isotope. This drastically increases the count rate of incoherent scattering [7]. The isotope selectivity allows one to avoid the influence of the substrate and the cover material.

Another type of material that cannot be obtained in large amounts are nanoparticles. Typically they are available in quantities of a few milligrams. Nevertheless, this is sufficient to investigate lattice dynamics using inelastic nuclear absorption [9,10]. An example is shown in figure 10. The energy spectrum of nuclear absorption in nanoparticles of α-iron is compared with that of a bulk iron sample [9]. α-iron nanoparticles of $\sim$10 nm size were prepared by ballistic consolidation. The energy spectrum of nuclear absorption for nanoparticles shows a large energy distortion relative to the bulk iron sample. It has long tails beyond 39 meV, above the energy cutoff for the bulk α-iron. This distortion was attributed to additional broadening of phonon modes due to a short phonon lifetime. In addition, an enhanced phonon density was observed below 15 meV. The total amount of material used in the experiment was only 4 mg.

The two above examples demonstrate the impressive potential of inelastic nuclear scattering, especially in those domains where it can efficiently compete with traditional techniques. Among other important applications under development one may note the

investigations of lattice dynamics in quasi-crystals [51], macromolecules [4,16,17], proteins [18–20], and experiments under high pressure [52].

8. Data treatment and obtained information

The main advantage of inelastic nuclear scattering is the direct access to the density of phonon states [2]. In this field it gives more precise and more reliable information than other inelastic techniques. In contrast to, e.g., incoherent inelastic neutron scattering, inelastic nuclear absorption provides an ideal averaging over phonon wave vectors, whereas with the neutron technique the approximation of incoherent scattering can never be precise due to incomplete covering of the solid angle by the detectors and due to the contribution of coherent scattering. As opposed to, e.g., coherent inelastic neutron or X-ray scattering, with inelastic nuclear scattering the density of phonon states is obtained directly from the experimental data, without any model of the lattice invoked. An assumption of harmonic vibrations, which has to be taken into account for treating multiphonon scattering, is not really essential, especially at low temperatures, when the one-phonon term is the dominating contribution.

Furthermore, compared to other techniques, inelastic nuclear scattering provides a more realistic description of the density of states. With coherent inelastic neutron scattering, for instance, the dispersion relations are treated as exact Dirac δ-functions $\delta[E - \hbar\omega(\vec{q})]$. In reality, however, they are "broadened" due to the finite lifetime of the phonons. Molecular-dynamic calculations show that a finite phonon lifetime should cause smoothing of the density of states. The effect may be significant even below room temperature [53]. In neutron scattering, the influence of the phonon lifetime is completely disregarded, whereas direct measurements of the density of states with nuclear scattering do reveal it. For instance, the data on the density of states in α-iron, which were obtained by the two techniques, are compared in figure 11. The data for inelastic nuclear absorption (open circles) are taken from [54], the measurements on the ^{57}Fe sample were carried out with 0.66 meV energy resolution. The data for neutron scattering (solid line) are based on [15], where the density of states for natural iron was obtained after fitting the experimental data of dispersion relations with a Born–von-Kármán fifth-neighbour general-force-constant model [55]. For an adequate comparison with nuclear absorption data, we convoluted the density of states from neutron measurements with a 0.66 meV wide Gaussian distribution. Figure 11 shows the good agreement of the density of states from the two techniques almost along the complete energy range. A slight shift of the nuclear absorption data to the lower frequencies is consistent with $\sim$1% isotope effect. However, a significant disagreement exists in the vicinity of 36 meV, where the neutron data have a sharper tip. In order to match both sets of data, one would need to convolute the neutron data with a Gaussian distribution of about 2.0 meV energy width. This additional broadening is completely outside the possible uncertainties of inelastic nuclear absorption. On the other hand, it exactly matches the typical broadening of the phonon modes at room temperature [56], which is not taken into account by the neutron data.

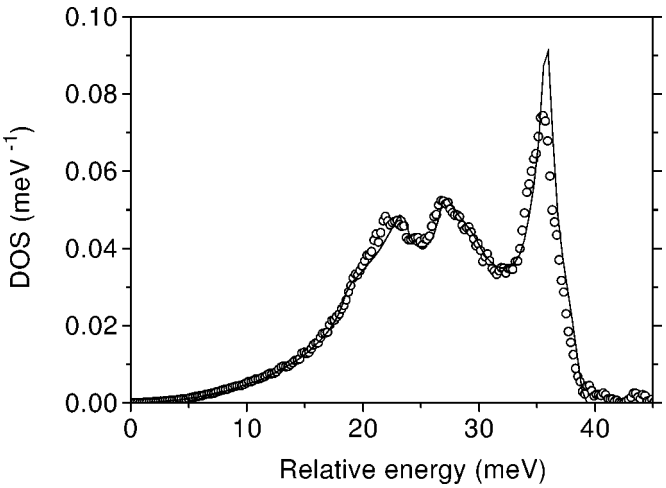

Figure 11. Comparison of the data on density of phonon states in α-iron, obtained with inelastic nuclear absorption (open circles, from [54]) and with inelastic neutron scattering (solid line, from [15]) techniques. The neutron data have been convoluted with a Gaussian instrumental function of 0.66 meV width.

The procedure of extracting the density of phonon states from the experimental data of inelastic nuclear absorption is governed by eqs. (5.1)–(5.3). It does not require any theoretical model or additional information other than experimental data. Normalization of the experimental data is achieved using the Lipkin sum rules [2]. The density of states is obtained from the one-phonon term of inelastic absorption $S_1(E)$ according to eq. (5.2). This term can be separated from the normalized spectrum of inelastic absorption $W(E)$ after subtraction of multi-phonon contributions with a recursive procedure according to eq. (5.3). This requires the Lamb–Mössbauer factor, which is obtained directly from the normalized experimental data according to the obvious relation

$$\int_{-\infty}^{-0} W(E)\,\mathrm{d}E + \int_{0}^{\infty} W(E)\,\mathrm{d}E = 1 - f_{\mathrm{LM}}. \tag{8.1}$$

In practice the experimental data are influenced by the finite energy resolution. In a first approximation, one may ignore this influence and treat the data as discussed above. Then one obtains the "smoothed" density of phonon states, which is described by eq. (5.4) with the Dirac δ-function $\delta(E)$ substituted by the normalized instrumental function of the high-resolution monochromator [30]. This approximation is simple and works well even for experimental data with a moderately low statistical accuracy. However, smoothing may be destructive because the density of states is not a slow function in general. Furthermore, treating the multi-phonon contributions according to eq. (5.3) is not exactly justified for the "un-convoluted" experimental data [30]. Therefore, application of some deconvolution procedure is desirable. This may be done using the forward and reversed Fourier transformations of the experimental data [30, 31,57]. In this approach the deconvolution is achieved by dividing the Fourier image

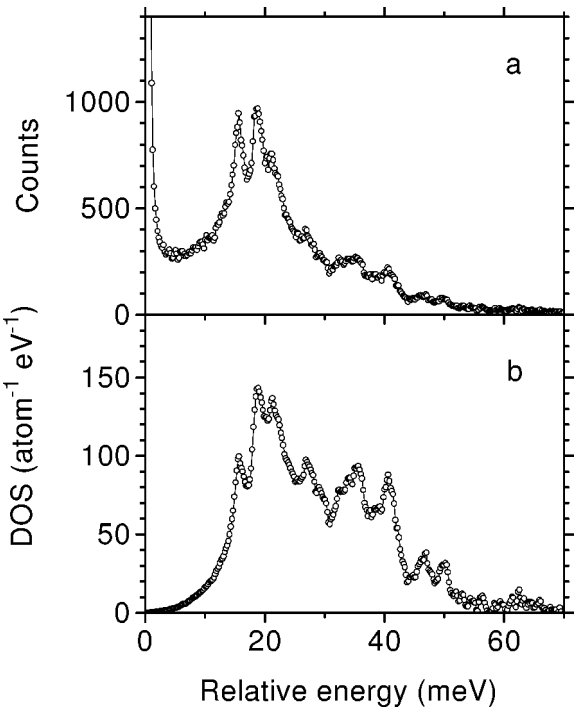

Figure 12. (a) Energy spectrum of inelastic nuclear absorption of synchrotron radiation in a hematite $^{57}Fe_2O_3$ sample, and (b) the derived density of phonon states. From [54].

of the experimental data by the Fourier image of the instrumental functions, and the logarithm of the obtained ratio separates the one-phonon term from the multi-phonon contributions.

By definition, the obtained density of states is a "partial" DOS, which corresponds to the vibrations of only the specific atoms of Mössbauer isotopes. If these atoms occupy several different sites of the lattice, their contributions to the DOS are weighted by the corresponding Lamb–Mössbauer factors [30,32].

An example of the raw experimental data and the derived density of states is presented in figure 12. Figure 12(a) shows the phonon-creation part of the energy spectrum of inelastic nuclear absorption in a single crystal of hematite $^{57}Fe_2O_3$. The spectrum was measured with 0.66 meV energy resolution [54]. The data were treated using the forward and reversed Fourier transformation [31]. The derived density of phonon states is shown in figure 12(b). It follows the $\sim E^2$ Debye approximation up to approximately 15 meV. At higher energies, several sharp peaks appear, which originate from those regions of the dispersion surface where the phonon frequency varies slowly with phonon momentum. The density of states has a cutoff at $\sim$52 meV, which indicates the proper elimination of the multi-phonon contributions.

Knowledge of the density of phonon states gives complete information on several important thermodynamical properties. For instance, the vibrational contribution to the

internal energy per atom (which takes into account the zero-point vibrations) may be found as [58]

$$U = \frac{3}{2}\int_0^\infty g(E)E\frac{\mathrm{e}^{\beta E}+1}{\mathrm{e}^{\beta E}-1}\,\mathrm{d}E. \tag{8.2}$$

Differentiating with respect to temperature and neglecting the temperature dependence of the density of states, one obtains the lattice specific heat per atom at constant volume as [58]

$$C_V = 3k_\mathrm{B}\int_0^\infty g(E)\frac{(\beta E)^2\mathrm{e}^{\beta E}}{(\mathrm{e}^{\beta E}-1)^2}\,\mathrm{d}E. \tag{8.3}$$

In order to obtain the lattice specific heat at constant pressure, one may use the relative variation of the mean frequency with temperature [14]. Then the lattice specific heat at constant pressure can be estimated as [59]

$$C_P = C_V\left(1 - T\frac{1}{\nu}\frac{\mathrm{d}\nu}{\mathrm{d}T}\right), \tag{8.4}$$

where ν is the mean vibrational frequency [59]. Comparison of the calculated lattice specific heat with the calorimetric data allows one to estimate the electronic contribution to the specific heat at high temperatures [4,59].

The vibrational entropy per atom can be found as [58]

$$S = 3k_b\int_0^\infty g(E)\left[\frac{\beta E}{2}\frac{\mathrm{e}^{\beta E}+1}{\mathrm{e}^{\beta E}-1} - \ln\bigl(\mathrm{e}^{\beta E/2}-\mathrm{e}^{-\beta E/2}\bigr)\right]\mathrm{d}E. \tag{8.5}$$

At high temperatures, the difference in vibrational entropy between two phases may be approximated as [9]

$$S_1 - S_2 = 3N_A k_\mathrm{B}\int_0^\infty \bigl(g_1(E) - g_2(E)\bigr)\ln(E)\,\mathrm{d}E. \tag{8.6}$$

The calculation of vibrational entropy allows one to conclude what drives the structural transformations [9].

Besides the density of phonon states, several properties may be obtained directly from the raw experimental data using the sum rules [47,48] for energy moments of the probability of inelastic absorption:

$$\bigl\langle (E-E_\mathrm{R})^n\bigr\rangle_W \equiv \int_{-\infty}^\infty W(E)(E-E_\mathrm{R})^n\,\mathrm{d}E. \tag{8.7}$$

As mentioned above, the sum rules for zero and first moments provide normalization of the experimental data. After subtraction of the central peak, the recoil fraction of nuclear scattering $1 - f_\mathrm{LM}$ may be found as an integral of the inelastic part ("zeroth moment") according to eq. (8.1). In general, this procedure does not give the exact value of the Lamb–Mössbauer factor but its upper bound, because the subtracted central peak may hide some unresolved quasielastic contribution to the scattering. In relevant

cases it is worth checking the balance by comparing the recoil fraction $1-f_{\mathrm{LM}}$ obtained from inelastic nuclear absorption with the recoilless fraction f_{LM} obtained from some other method, for instance, from nuclear forward scattering. The lower bound for the Lamb–Mössbauer factor may be obtained by applying eq. (8.1) to the normalized experimental data without subtraction of the central peak [32,42]. From the Lamb–Mössbauer factor, the atomic mean-square displacements can be calculated according to

$$\left\langle \Delta x^2 \right\rangle = -\frac{\ln(f_{\mathrm{LM}})}{k^2}. \tag{8.8}$$

From the higher order moments, one can obtain the mean kinetic energy $T(\vec{s})$ and the mean force constant $V(\vec{s})$ along the direction $\vec{s}$ of the incident X-ray beam as [48]

$$T\left(\vec{s}\right) = \frac{1}{4E_{\mathrm{R}}}\left\langle (E-E_{\mathrm{R}})^2 \right\rangle_W, \tag{8.9}$$

$$V\left(\vec{s}\right) = \frac{M}{\hbar^2 E_{\mathrm{R}}}\left\langle (E-E_{\mathrm{R}})^3 \right\rangle_W. \tag{8.10}$$

From the mean kinetic energy, the second-order Doppler shift can be derived and compared with the data from conventional Mössbauer spectroscopy [32]. The mean force constant in harmonic approximation should not depend on temperature, hence, it offers a tool to reveal the anharmonicity of lattice vibrations. The measurements of the Lamb–Mössbauer factor and the second-order Doppler shift are reviewed in detail in [32].

The values obtained from the sum rules can alternatively be recalculated using the derived density of states. This gives a useful possibility to check the reliability of the experimental data and the correctness of the data treatment [14]. For instance, the Lamb–Mössbauer factor may be calculated according to eq. (6.2) and compared to that from eq. (8.1). The proper normalization of the derived DOS may be checked. The procedure can also be extended to higher moments [30]. For instance, the mean kinetic energy and the mean force constant along the direction $\vec{s}$ of the incident X-ray beam can be found as [30]

$$T\left(\vec{s}\right) = \frac{1}{4}\int_0^\infty \tilde{g}\left(E,\vec{s}\right) E \frac{\mathrm{e}^{\beta E}+1}{\mathrm{e}^{\beta E}-1}\,\mathrm{d}E, \tag{8.11}$$

$$V\left(\vec{s}\right) = \frac{M}{\hbar^2}\int_0^\infty \tilde{g}\left(E,\vec{s}\right) E^2\,\mathrm{d}E \tag{8.12}$$

and compared with the calculations according to eqs. (8.9) and (8.10). In accordance with an assumption of the harmonic vibrations, the total (summed over all directions) mean kinetic energy is equal to half the vibrational internal energy (eq. (8.2)).

9. Nuclear resonance energy analysis of inelastic X-ray scattering

Nuclear inelastic absorption is only sensitive to the vibrations of the Mössbauer nuclei; therefore, it provides the partial density of states of the selected atoms in the unit cell. Thus inelastic nuclear scattering is an isotope-selective technique, because the "instrument" for the energy analysis is a "built-in" feature of the selected atoms. One may, however, separate the "instrument" and the "sample" and use the nuclear resonance in order to analyze the energy of radiation scattered by the non-Mössbauer atoms [21].

The experimental setup for these measurements is shown in figure 13. The sample no longer has to contain the resonant nuclei. Resonance analysis of the scattered radiation is performed by the detector, which has the foil of the resonant isotope in front of the window. The quanta experience inelastic X-ray scattering by the sample and irradiate the resonant foil. If in the scattering process the energy of the X-ray quantum is shifted to match the energy of the nuclear resonance, this event produces the delayed signal in the detector. The second detector, as in the previous setup (figure 1), measures the instrumental function of the monochromator.

In this setup the resonance detector should serve as an ideal energy analyzer, i.e., the delayed signal should only be produced if the energy of the scattered quantum coincides precisely with the resonance energy. Therefore, any effect of inelastic nuclear absorption in the resonant foil should be avoided. This is achieved with a thin filter between the resonant foil and the detector. The filter absorbs the low-energy atomic fluorescence but is mostly transparent for the resonant radiation. Therefore the delayed signal results only from the elastic process of forward nuclear scattering in the resonant foil. The contribution of inelastic nuclear scattering, which results in incoherent emission of nuclear fluorescence, is usually negligible due to radiation trapping [34].

An example of nuclear resonance energy analysis of inelastic X-ray scattering is shown in figure 14. The energy distributions of X-rays scattered by water, Plexiglas, and gaseous xenon were measured [21]. The presence of inelastic scattering is clearly seen in a considerable broadening and in long tails of the energy spectra of scattered radiation relative to the instrumental function (dashed lines). The solid lines show the fit to the experimental data using a phenomenological approach (a), the density of

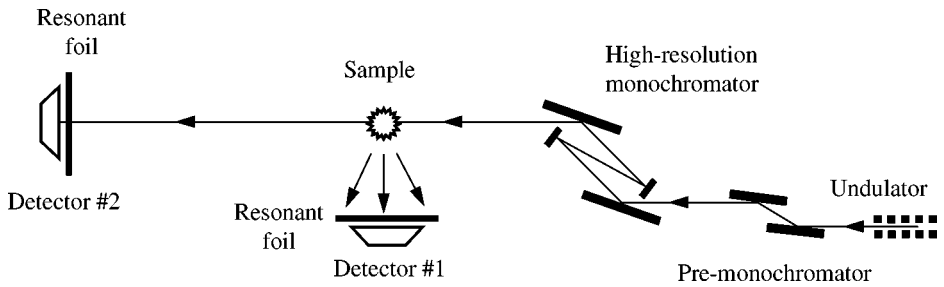

Figure 13. Experimental setup for the measurements of inelastic X-ray scattering with nuclear resonant energy analysis of the scattered radiation.

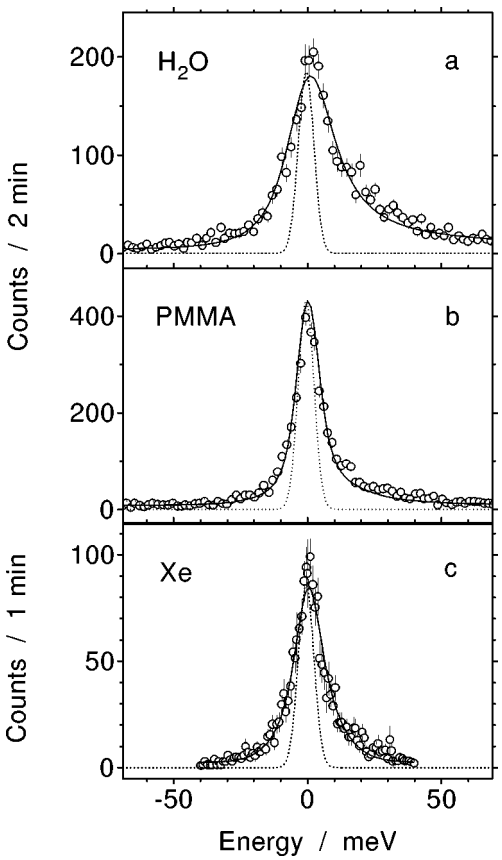

Figure 14. Energy spectra of inelastic X-ray scattering by water, PMMA, and gaseous Xe. The dashed lines show the instrumental function. The solid lines are the fit to the experimental data. From [21].

states obtained in neutron studies (b), and a Doppler broadening model (c) (see [21] for the details).

The experimental setup of nuclear inelastic scattering (figure 1) and inelastic X-ray scattering with nuclear resonance analysis (figure 13) are almost identical. This allows one to investigate the dynamics of both Mössbauer and non-Mössbauer atoms and to obtain the site-selective and the site-averaged spectra of lattice vibrations in the same experiment. The comparison is especially valuable for samples with complicated lattices (e.g., proteins), where the vibrations of the resonant atoms differ considerably from the "averaged" vibrations of the lattice [18–20,60].

10. Summary

Inelastic nuclear scattering shows an impressive development, having passed from first observations to an elaborate experimental technique in only a few years. A relatively simple experimental setup, high precision, and short measuring time provide a

good basis for an increasing number of applications. The most convincing success has been achieved for non-crystalline phases and in experiments with small amounts of material, where the new technique has distinct advantages over traditional methods. In summary, nuclear inelastic scattering will probably become one of the most powerful techniques to study the dynamics of matter.

Acknowledgements

W.S. is indebted to E.E. Alp, T.S. Toellner, M.Y. Hu, P.M. Hession, and J. Sutter of the Advanced Photon Source at Argonne National Laboratory for support during experiments and fruitful discussions. A.C. thanks his colleagues from the Nuclear Resonance group at the European Synchrotron Radiation Facility for their help and V. Kohn from the Russian Research Center Kurchatov Institute in Moscow for helpful discussions. Use of the Advanced Photon Source was supported by the U.S. Department of Energy, Basic Energy Sciences, Office of Science, under Contract No. W-31-109-Eng-38.

References

[1] M. Seto, Y. Yoda, S. Kikuta, X.W. Zhang and M. Ando, Phys. Rev. Lett. 74 (1995) 3828.
[2] W. Sturhahn, T.S. Toellner, E.E. Alp, X.W. Zhang, M. Ando, Y. Yoda, S. Kikuta, M. Seto, C.W. Kimball and B. Dabrowski, Phys. Rev. Lett. 74 (1995) 3832.
[3] A.I. Chumakov, R. Rüffer, H. Grünsteudel, H.F. Grünsteudel, G. Grübel, J. Metge, O. Leupold and H.A. Goodwin, Europhys. Lett. 30 (1995) 427.
[4] A.I. Chumakov and R. Rüffer, Hyp. Interact. 113 (1998) 59.
[5] E.E. Alp, W. Sturhahn, T. Toellner, P. Lee, M. Schwoerer-Böhning, M. Hu, P. Hession, J. Sutter and P. Abbamonte, Adv. Photon Source Resarch 1, ANL/APS/TB-31 (1998) 9.
[6] W. Keune and W. Sturhahn, this issue, section V-1.5.
[7] R. Röhlsberger, W. Sturhahn, T.S. Toellner, K.W. Quast, E.E. Alp, A. Bernhard, J. Metge, R. Rüffer and E. Burkel, Phys. B 263–264 (1999) 581.
[8] W. Sturhahn, R. Röhlsberger, E.E. Alp, T. Ruckert, T. Schrör and W. Keune, J. Magn. Magn. Mater. 198–199 (1999) 590.
[9] B. Fultz, C.C. Ahn, E.E. Alp, W. Sturhahn and T.S. Toellner, Phys. Rev. Lett. 79 (1997) 937.
[10] S. Kikuta, Y. Yoda, I. Kojama, T. Shimizu, H. Igarashi, K. Izumi, Y. Kunimune, M. Seto, T. Mitsui, T. Harami, X. Zhang and M. Ando, in: *X-ray and Inner-Shell Processes, Proc. of the 17th Internat. Conf.*, eds. R.L. Johnson, H. Schmidt-Böcking and B.F. Sonntag, AIP Conf. Proc., Vol. 389, Woodbury, NY (1996) p. 351.
[11] X.W. Zhang, Y. Yoda, M. Seto, Yu. Maeda, M. Ando and S. Kikuta, Japan J. Appl. Phys. 34 (1995) L330.
[12] A.Q.R. Baron, A.I. Chumakov, S.L. Ruby, J. Arthur, G.S. Brown, G.V. Smirnov and U. van Bürck, Phys. Rev. B 51 (1995) 16384.
[13] B. Fultz, T.A. Stephens, W. Sturhahn, T.S. Toellner and E.E. Alp, Phys. Rev. Lett. 80 (1998) 3304.
[14] A.I. Chumakov, R. Rüffer, A.Q.R. Baron, H. Grünsteudel and H.F. Grünsteudel, Phys. Rev. B 54 (1996) 9596.
[15] H.R. Schober and P.H. Dederichs, in: *Phonon States of Elements. Electron States and Fermi Surfaces of Alloys*, Landolt–Börnstein, Vol. III/13a, eds. K.-H. Hellwege and J.L. Olsen (Springer, Berlin, 1981) p. 56.

[16] R. Rüffer and A.I. Chumakov, Hyp. Interact. 97/98 (1996) 589.
[17] H. Grünsteudel, H. Paulsen, W. Mayer-Klaucke, H. Winkler, A.X. Trautwein, H.F. Grünsteudel, A.Q.R. Baron, A.I. Chumakov, R. Rüffer and H. Toflund, Hyp. Interact. 113 (1998) 311.
[18] C. Keppler, K. Achterhold, A. Ostermann, U. van Bürck, W. Potzel, A.I. Chumakov, A.Q.R. Baron, R. Rüffer and F. Parak, European Biophys. J. 25 (1997) 221.
[19] T. Harami, G. Mijazaki, M. Seto, T. Mitsui, Y. Yoda, Y. Kobajashi, S. Kitao and X.W. Zhang, Hyp. Interact. C 3 (1998) 61.
[20] F. Parak and K. Achterhold, this issue, section V-1.3.
[21] A.I. Chumakov, A.Q.R. Baron, R. Rüffer, H. Grünsteudel, H.F. Grünsteudel and A. Meyer, Phys. Rev. Lett. 76 (1996) 4258.
[22] Internet page `http://www.esrf.fr/exp_facilities/ID18/handbook/handbook.html`.
[23] Internet page `http://www.aps.anl.gov/sricat/3id.html`.
[24] E.E. Alp, T.M. Mooney, T. Toellner and W. Sturhahn, Hyp. Interact. 90 (1994) 323.
[25] Internet page `http://www.spring8.or.jp/ENGLISH/facility/bl/PublicBeamline/BL09XU/index.html`.
[26] J.-L. Revol, E. Plouviez and R. Rüffer, Synchrotron Radiation News 7(4) (1994) 23.
[27] T.S. Toellner, this issue, section VI-1.
[28] A.I. Chumakov, R. Rüffer, A.Q.R. Baron, J. Metge, H. Grünsteudel and H.F. Grünsteudel, in: *SPIE Proceedings*, 3151, ed. A.T. Macrander (1997) p. 262.
[29] A.Q.R. Baron, this issue, section VI-2.
[30] V.G. Kohn, A.I. Chumakov and R. Rüffer, Phys. Rev. B 58 (1998) 8437.
[31] M.Y. Hu, W. Sturhahn, T.S. Toellner, P.M. Hession, J.P. Sutter and E.E. Alp, Nucl. Instrum. Methods A (1999) in press.
[32] W. Sturhahn and A.I. Chumakov, this issue, section V-1.2.
[33] A.Q.R. Baron, A.I. Chumakov, R. Rüffer, H. Grünsteudel, H.F. Grünsteudel and O. Leupold, Europhys. Lett. 34 (1996) 331.
[34] A.I. Chumakov, J. Metge, A.Q.R. Baron, R. Rüffer, Yu.V. Shvydko, H. Grünsteudel and H.F. Grünsteudel, Phys. Rev. B 56 (1997) 8455.
[35] W. Sturhahn and V. Kohn, this issue, section III-2.2.
[36] U. van Bürck, this issue, section IV-2.1.
[37] G.V. Smirnov and V.G. Kohn, Phys. Rev. B 52 (1995) 3356.
[38] W. Sturhahn, K.W. Quast, T.S. Toellner, E.E. Alp, J. Metge and E. Gerdau, Phys. Rev. B 53 (1996) 171.
[39] A.I. Chumakov, J. Metge, A.Q.R. Baron, H. Grünsteudel, H.F. Grünsteudel, R. Rüffer and T. Ishikawa, Nucl. Instrum. Methods A 383 (1996) 642.
[40] T.S. Toellner, M.Y. Hu, W. Sturhahn, K. Quast and E.E. Alp, Appl. Phys. Lett. 71 (1997) 2112.
[41] J. Metge, Ph.D. thesis, Universität Hamburg (1996).
[42] A.I. Chumakov, A. Barla, R. Rüffer, J. Metge, H.F. Grünsteudel, H. Grünsteudel, J. Plessel, H. Winkelmann and M.M. Abd-Elmeguid, Phys. Rev. B 58 (1998) 254.
[43] B. Sepiol, A. Meyer, G. Vogl, R. Rüffer, A.I. Chumakov and A.Q.R. Baron, Phys. Rev. Lett. 76 (1996) 3220.
[44] K.S. Singwi and A. Sjölander, Phys. Rev. 120 (1960) 1093.
[45] E.G. Brovman and Yu. Kagan, Fizika Tverdogo Tela 8 (1966) 1402. (Soviet Phys. Solid State 8 (1966) 1120).
[46] M. Seto, Y. Yoda, S. Kikuta, X.W. Zhang and M. Ando, Il Nuovo Cimento D 18 (1996) 381.
[47] H.J. Lipkin, Ann. Phys. (NY) 9 (1960) 332.
[48] H.J. Lipkin, Phys. Rev. B 52 (1995) 10073.
[49] A.I. Chumakov, R. Rüffer, A.Q.R. Baron, H. Grünsteudel, H.F. Grünsteudel and V.G. Kohn, Phys. Rev. B 56 (1997) 10 758.

[50] P.M. Hession, W. Sturhahn, E.E. Alp, T.S. Toellner, P. Metcalf, M.Y. Hu, J.P. Sutter and J.P. Mullen, Argonne National Laboratory, in preparation.
[51] R. Brand et al., Phys. Rev. B 59 (1999) 14145.
[52] R. Lübbers, M. Pleines, G. Wortmann, H.F. Grünsteudel and R. Rüffer, ESRFs User Report No. HS-583 (1998) (Internet page `http://www.esrf.fr/info/science/annrep/usrrep.html`).
[53] J.M. Dickey and A. Paskin, Phys. Rev. 188 (1969) 1407.
[54] T.S. Toellner et al., Argonne National Laboratory (1997) unpublished.
[55] V.J. Minkiewicz, G. Shirane and R. Nathans, Phys. Rev. 162 (1967) 528.
[56] J. Menéndez and M. Cardona, Phys. Rev. B 29 (1984) 2051.
[57] D.W. Johnson and J.C.H. Spence, J. Phys. D Appl. Phys. 7 (1974) 771.
[58] W. Jones and N.H. Marsh, *Theoretical Solid State Physics*, Vol. 1 (Dover, New York, 1985) p. 237.
[59] A.P. Miller and B.N. Brockhouse, Canad. J. Phys. 49 (1971) 704.
[60] K. Achterhold, C. Keppler, U. van Bürck, W. Potzel, P. Schindelmann, E.-W. Knapp, B. Melchers, A.I. Chumakov, A.Q.R. Baron, R. Rüffer and F. Parak, European Biophys. J. 25 (1996) 43.